

Self-Calibrated CLIP for Training-Free Open-Vocabulary Segmentation

Sule Bai*, Yong Liu*, Yifei Han, Haoji Zhang, Yansong Tang[†]
 Tsinghua Shenzhen International Graduate School, Tsinghua University

{bs123, liuyong23}@mails.tsinghua.edu.cn, tang.yansong@sz.tsinghua.edu.cn

Abstract

Recent advancements in pre-trained vision-language models like CLIP, have enabled the task of open-vocabulary segmentation. CLIP demonstrates impressive zero-shot capabilities in various downstream tasks that require holistic image understanding. However, due to its image-level pre-training, CLIP struggles to capture local details, resulting in poor performance in segmentation tasks. Our analysis reveals that anomaly tokens emerge during the forward pass, drawing excessive attention from normal patch tokens, thereby diminishing spatial awareness. To address this issue, we propose Self-Calibrated CLIP (SC-CLIP), a training-free method that calibrates CLIP to produce finer-grained representations while preserving its original generalization ability, without introducing new parameters or relying on additional backbones. Specifically, we first identify and resolve the anomaly tokens to mitigate their negative impact. Next, we enhance feature discriminability and attention correlation by leveraging the semantic consistency found in CLIP’s intermediate features. Furthermore, we employ multi-level feature fusion to enrich details. Collectively, these strategies enhance CLIP’s feature representation with greater granularity and coherence. Experimental results demonstrate the effectiveness of SC-CLIP, achieving state-of-the-art results across eight semantic segmentation datasets and surpassing previous methods by 9.5%. Notably, SC-CLIP boosts the performance of vanilla CLIP ViT-L/14 by 6.8 times. Our source code is available [here](#).

1. Introduction

Open-Vocabulary Segmentation (OVS) is an emerging task in computer vision that aims to segment arbitrary categories based on the textual inputs, overcoming the limitations of predefined category sets. To achieve this, models must generalize beyond the training data. Vision-language pretrained models such as CLIP [39], demonstrate remarkable zero-shot capabilities by leveraging large-scale image-text pairs,

*Equal contribution

[†]Corresponding author

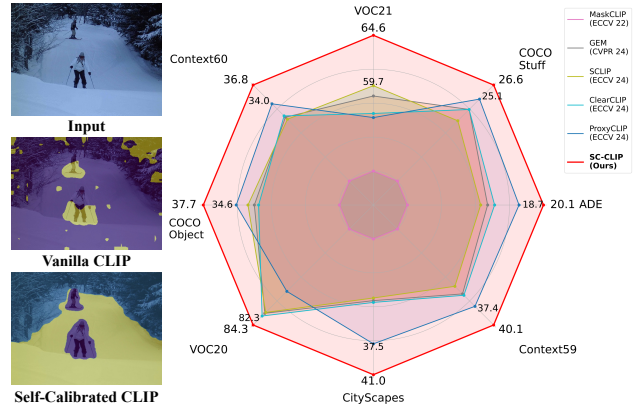


Figure 1. Left: Vanilla CLIP produces a noisy segmentation map, while our Self-Calibrated CLIP (SC-CLIP) generates a clearer and finer result. Right: Comparison of the open-vocabulary segmentation performance, where SC-CLIP achieves the best results.

effectively fulfilling these requirements. However, CLIP’s image-text matching strategy leads to an excessive emphasis on global context, neglecting local and fine-grained details essential for dense prediction tasks. Consequently, directly applying CLIP to segmentation tasks yields poor performance. For example, as shown in Figure 1, the segmentation result generated by patch-text cosine similarity exhibits considerable noise. CLIP ViT-B/16 achieves only 8.9% mIoU on the COCO-Object dataset [6], significantly lagging behind its ability on image-level recognition.

To address CLIP’s limitations in capturing local details, recent studies have proposed various modifications to its last layer. One line of research [4, 18, 22, 25, 29, 42, 46, 61] introduces correlative attention, replacing the original Q-K attention with alternatives like K-K, to enhance focus on relevant regions. But these methods still operate on the global and noisy inputs, hindering their effectiveness. Another approach [26, 48] incorporates additional backbones [7, 24, 41] to provide richer spatial details. Despite performance gains, they fail to fully exploit CLIP’s semantic knowledge and impose extra computational costs. In fact, both strategies overlook the underlying causes of CLIP’s global focus, preventing them from fundamentally resolving the issue of diminished spatial awareness in CLIP.

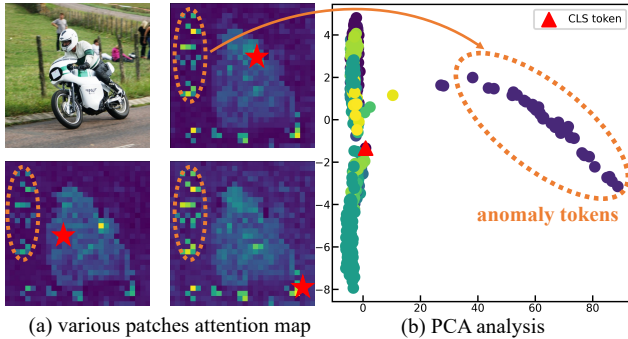


Figure 2. Anomaly tokens in CLIP. (a) visualizes the attention map of various selected patches (marked by \star), all exhibit excessive focus on the same regions (indicated by orange circle), aligning with the identified outliers in the PCA analysis in (b).

Motivated by this, we begin with an in-depth analysis of CLIP. As indicated by the orange circles in Figure 2 (a), we observe that different patch tokens consistently exhibit high activation regions within their attention map. These tokens attract excessive attention from other normal patches, distracting their focus away from local and relevant areas. To further investigate, we apply PCA [1] analysis to CLIP’s features in Figure 2 (b), revealing these over-attended tokens differ significantly from the normal ones (including the [CLS] token). Thus, we refer to them as anomaly tokens. We attribute CLIP’s disadvantage in dense prediction tasks to the emergence of anomaly tokens, which leads to uniform attention activations across locations. This disrupts the attention’s ideal ability to extract relevant semantics, resulting in representation smoothing that diminishes local awareness and further exacerbates disorganization in the feature maps.

Building on the analysis, we propose enhancing CLIP’s feature representation by weakening the influence of anomaly tokens. To achieve this, we introduce Self-Calibrated CLIP (SC-CLIP), a training-free approach that leverages CLIP’s inherent properties for effective calibration, strengthening its perception on local and relevant regions. On the one hand, we propose directly resolving these anomaly tokens. To identify them, we apply the Local Outlier Factor (LOF) algorithm [5], a method for detecting outliers. Once located, we replace these anomaly tokens with values interpolated from their spatial neighbors, considering that spatially close regions often share similar semantics. This not only serves as a regularization to prevent inappropriate attention focus but also reassigns meaningful semantic information to the anomaly tokens, aligning them with the local context. On the other hand, to mitigate the feature smoothing problem caused by anomaly tokens, we propose a self-adjusting strategy to enhance features’ local discriminability and attention correlation. We observe that the intermediate layers’ features of CLIP exhibit good semantic coherence, as shown in Figure 4. In order to retain the rich semantics of deep features and the spatial consistency of

intermediate features, we utilize the latter to adaptively aggregate deep features, while simultaneously enhancing attention correlation. This self-adjusting approach improves the feature’s semantic coherence. Furthermore, we explore a multi-level feature fusion strategy to complement CLIP’s capabilities in dense prediction tasks, facilitating a better capture of feature details at different scales.

Experimental results demonstrate that SC-CLIP achieves remarkable performance, establishing new state-of-the-art results across eight datasets, as shown in Figure 1. Our approach significantly outperforms previous methods by 9.5% on CLIP ViT-B/16. Notably, SC-CLIP boosts the performance of vanilla CLIP ViT-L/14 by 6.8 times, without the need for additional parameters, data, or backbones.

Our contributions can be summarized as follows:

- We propose SC-CLIP, a training-free method designed to enhance CLIP’s dense feature representation, effectively addressing the uniform attention activations and feature smoothing caused by the anomaly tokens.
- We calibrate CLIP with its inherent properties. Specifically, we propose resolving the anomaly tokens and mitigate their negative impact. And we utilize the spatial consistency in CLIP’s mid-level features to enhance feature discriminability and attention correlation.
- Our approach sets new state-of-the-art results across popular benchmarks. And we conduct extensive experiments to validate the effectiveness of our method.

2. Related Work

Vision-Language Pre-training. Vision-language models [21, 28, 39] pretrained on large-scale web data, represented by CLIP [39], employ contrastive learning to align images with associated captions, demonstrating remarkable zero-shot capabilities across a wide range of downstream tasks that require holistic image understanding [2, 23, 35]. However, CLIP’s image-level pre-training, which relies on the [CLS] token to represent the whole image, causes the model to overly focus on global features at the expense of local and fine-grained details. This limitation hinders its performance in dense prediction tasks which require pixel-level understanding. To address this, our work focuses on effectively adapting CLIP for segmentation task while preserving its original knowledge and cross-modal capabilities.

Open-Vocabulary Segmentation. The open-vocabulary segmentation (OVS) task focuses on segmenting images with arbitrary text queries by leveraging the zero-shot capabilities of vision-language models [21, 39]. Existing works can be broadly classified into three categories: fully-supervised, weakly-supervised and training-free. Fully-supervised methods [9, 13, 16, 19, 27, 31, 33, 38, 50, 54–58] require fine-tuning on pixel-level annotated datasets. Weakly-supervised approaches [8, 20, 34, 37, 40, 52, 53,

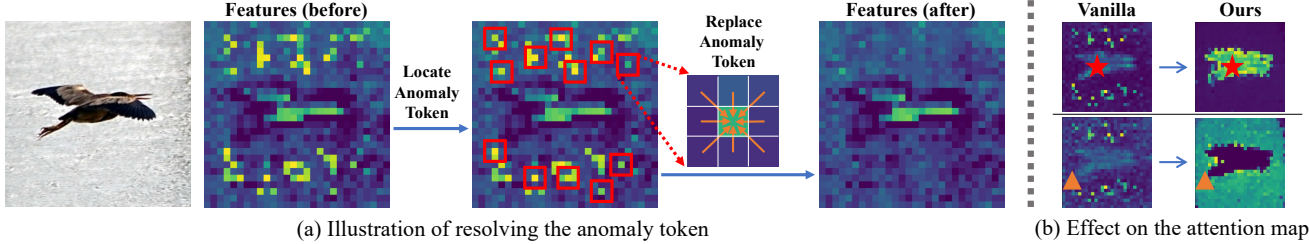


Figure 3. Resolving the Anomaly Tokens. (a) Illustration of the resolving process. We plot the feature map using the mean value of each token. After locating the anomaly tokens (the center of red square), we replace them with the interpolated values obtained from their neighboring regions. (b) Effect on the attention map. We highlight the changes for a normal token (★), and an anomaly token (▲).

59] reduce reliance on dense annotations by using image-text pair to guide region grouping. Training-free methods [3, 4, 18, 22, 26, 29, 42, 46, 48, 61] directly utilize CLIP for segmentation by making minimal adjustments to the model’s architecture without additional training.

Our approach needs no training and falls into the third category. Recent methods have discovered that CLIP’s final-layer exhibits poor spatial consistency and proposed various modifications. For instance, SCLIP [46] replaces the original Q-K attention with the Q-Q and K-K attention, to enhance correlation. ClearCLIP [25] identifies the noise mainly stems from the residual connections, and proposes to remove it. CLIPTrase [42] proposes using self-self attention along with clustering for post-processing. Other works leverage vision models like DINO [7] and SAM [24] for providing details. For example, CLIP-DINOiser [48] refines feature maps using the affinity learned from DINO’s feature correspondence, while ProxyCLIP [26] applies them to adjust attention weights. In contrast, our approach improves semantic coherence by exploiting CLIP’s internal properties and explicitly resolving the anomaly tokens.

3. Method

In this section, we begin with an overview of CLIP and its dense inference pipeline. We then present SC-CLIP, our approach aimed to enhance CLIP’s representation. First, we identify and mitigate the impact of anomaly tokens. Next, we utilize the mid-level features with spatial consistency to adaptively aggregate the deep features, while simultaneously enhancing attention correlation. Besides, we employ multi-level feature to capture details across various scales.

3.1. Preliminaries

CLIP ViT model encodes an input image into a token sequence $\mathbb{X} = [x_{\text{cls}}, x_1, \dots, x_N]$, where x_{cls} is the [CLS] token and the others represent dense visual features, comprising N patch tokens. The CLIP model includes multiple layers, with each layer l processing the input $\mathbb{X}^{(l-1)}$ as follows:

$$\mathbb{Z}^l = \text{SA}(\text{LN}(\mathbb{X}^{(l-1)})) + \mathbb{X}^{(l-1)} \quad (1)$$

$$\mathbb{X}^l = \text{FFN}(\text{LN}(\mathbb{Z}^l)) + \mathbb{Z}^l \quad (2)$$

where SA, FFN and LN denote self-attention module, feed-forward network, and layer normalization, respectively.

For dense inference, the visual features are aligned with C categories to produce the patch-text similarity map of dimensions $N \times C$. And the final segmentation result is obtained by applying argmax operation to this similarity map.

It is essential to note that CLIP’s image-level pretraining utilizes the [CLS] token to represent the entire image, which enables robust global feature capture but limits the model’s ability to perceive local details essential for dense prediction. Consequently, directly applying the CLIP model to dense prediction tasks yields suboptimal performance.

Our approach focuses on modifying the last layer of the CLIP visual encoder, while keeping the other layers unchanged to prevent model collapse. For clarity and consistency in notation, we denote $\mathbb{X}^{\text{penul}}$ and \mathbb{X}^{last} as the penultimate and last feature representations, respectively.

3.2. Resolving the Anomaly Tokens

We attribute CLIP’s limitations in dense prediction tasks to the presence of anomaly tokens within its features, which differ significantly from normal tokens. These anomaly tokens cause other tokens to disproportionately focus on them in deep layers, leading to identical activation regions, which undermines attention’s capacity to extract semantically coherent features. Since attention [14, 45] manages spatial arrangements, this pattern intensifies disorganization in the feature map, resulting in suboptimal performance. Studies [12, 42, 49] suggest that pretrained models like CLIP may identify redundant tokens and use them to gather global information, thereby expediting processing. However, these tokens lack semantics, conveying minimal information about their original positions.

To address the negative impact of anomaly tokens, we propose an intuitive approach to resolve them in $\mathbb{X}^{\text{penul}}$ before the last layer, as illustrated in Figure 3 (a). First, it is essential to identify the anomaly tokens. As previously analyzed, anomaly tokens exhibit a clear distinction from other tokens. To detect these anomalies, we apply the LOF (Local Outlier Factor) algorithm [5], a popular anomaly detection method that identifies outliers by measuring the local density deviation of data points relative to their neighbors.

Once the anomalies are located, we replace them with the values interpolated from their 3×3 neighboring regions, based on the assumption that features in spatially adjacent regions are generally similar. Specifically, we apply a 3×3 convolution kernel with the center set to 0. And if neighboring regions contain any other anomaly tokens, they are excluded from the interpolation. The operation’s formula is provided below, where $\tilde{\mathbb{X}}^{penul}$ denotes the feature after operation and \mathcal{A} is the set of anomaly tokens.

$$\tilde{\mathbb{X}}_{(x,y)}^{penul} = \frac{\sum_{i=-1}^1 \sum_{j=-1}^1 w_{i,j} \cdot \mathbb{X}_{(x+i,y+j)}^{penul}}{\sum_{i=-1}^1 \sum_{j=-1}^1 w_{i,j}}, \quad \forall (x,y) \in \mathcal{A}$$

$$w_{i,j} = \begin{cases} 0, & \text{if } (x+i, y+j) \in \mathcal{A} \\ 1, & \text{otherwise} \end{cases} \quad (3)$$

We believe that eliminating anomaly tokens offers two key benefits. First, it acts as a form of regularization for the attention. Second, it reassigns semantic information to these anomaly tokens, aligning them with the local context. As shown in the Figure 3 (b), the vanilla attention in CLIP has two issues: 1) normal tokens excessively focus on anomaly tokens, reducing attention on relevant local areas, and 2) anomaly tokens focus on prominent objects and other anomaly tokens. After resolving the anomaly tokens via interpolation, normal tokens refocus on relevant local regions, while the updated anomaly tokens also shift attention to appropriate areas. In summary, our method reduces the impact of anomaly tokens and enhances attention correlation.

3.3. Self-Adjusting for Semantic Coherence

After resolving the anomaly tokens, the model reduces focus on them in the last layer’s attention. However, a challenge still remains: anomaly tokens have already caused substantial disruption to the other normal tokens in the previous layers, diminishing their local awareness.

To enhance feature discriminability and correlation, some methods [26, 48] leverage backbones with strong spatial coherence like DINO [7], to provide fine-grained details. Although this approach improves performance, it introduces an additional backbone and incurs extra computational costs during either the training or testing phase. Moreover, they do not fully utilize CLIP’s semantic knowledge and may even impair its generalization capability.

This prompts us to explore whether such semantic coherence can be uncovered within CLIP itself. We begin by visualizing the patch similarities, as shown in Figure 4, where we observe the CLIP’s last layer performs poorly as expected. However, the mid-layer of CLIP exhibits stronger semantic coherence, comparable to that of DINO. Next, we quantitatively evaluate all features of CLIP. Using the ADE20K dataset [60], we extract patches from each layer l and compute cosine similarity between them to create the similarity map $\mathbf{Simi}^l \in \mathbb{R}^{N \times N}$, defined as $\mathbf{Simi}^l =$

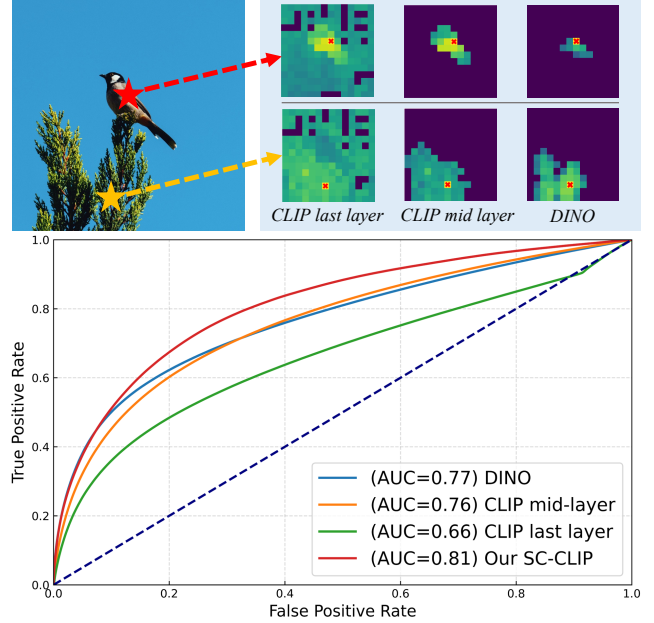


Figure 4. Top: Visualization of patch similarities, showing that CLIP’s deep layers perform poorly, but its mid-level layers exhibit semantic consistency comparable to DINO. Bottom: ROC curve analysis further supports this observation, with our SC-CLIP demonstrating superior semantic coherence.

$\frac{\mathbb{X}^l \cdot \mathbb{X}^l}{\|\mathbb{X}^l\| \|\mathbb{X}^l\|}$. This similarity map could serve as a binary classifier to indicate whether two patches belong to the same category, with patches of the same category labeled as 1 and otherwise 0. Each patch’s category is determined by majority voting on pixel labels in the segmentation map. For comparison, we also evaluate DINO [7]. To assess semantic coherence, we use ROC curve, where a higher area under the curve (AUC) reflects better semantic consistency. Results in Figure 4 show that CLIP’s mid-layer features \mathbb{X}^{mid} maintain strong spatial consistency (AUC=0.76), even comparable to DINO (AUC=0.77). However, CLIP’s last feature \mathbb{X}^{last} perform much worse (AUC=0.66).

The OVS task requires spatially coherent cross-modal alignment. CLIP’s last feature \mathbb{X}^{last} offers rich semantics but lacks coherence, while its mid-level features \mathbb{X}^{mid} exhibit strong spatial consistency but are semantically limited. To effectively combines the strengths of both, we propose a self-adjusting strategy as illustrated in Figure 5 (a). Specifically, we leverage \mathbf{Simi}^{mid} to adaptively aggregate \mathbb{X}^{deep} , generating new features $\hat{\mathbb{X}}^{deep}$ by combining semantically similar patches with weighted contributions based on their similarity. This process can be formulated as follows:

$$\hat{\mathbb{X}}_p^{deep} = \sum_{q=1}^N \text{Norm}(\mathbf{Simi}_{(p,q)}^{mid}) \cdot \mathbb{X}_q^{deep} \quad (4)$$

$$\text{Norm}(\mathbf{Simi}_{(p,\cdot)}^{mid}) = \frac{\mathbf{Simi}_{(p,\cdot)}^{mid}}{\sum_{r=1}^N \mathbf{Simi}_{(p,r)}^{mid}} \quad (5)$$

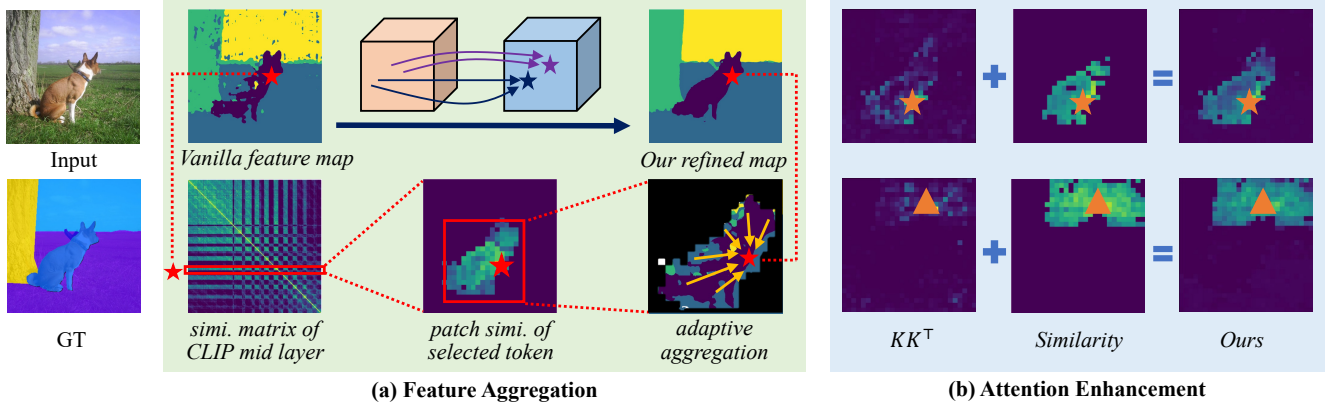


Figure 5. Illustration of the self-adjusting strategy. (a) We use the similarity map from CLIP’s mid layer to adaptively aggregate deep features by combining semantically similar patches, resulting in a clearer segmentation map. The second row provides a detailed view of the process for the selected patch \star . (b) We apply the similarity map to enhance attention, broadening and refining the activation regions.

The aggregated features $\hat{\mathbb{X}}^{deep}$ shows a clearer and more precise segmentation results, and a notable improvement in semantic coherence, with AUC increasing from 0.66 to 0.81 as shown in Figure 4 (Our SC-CLIP). This demonstrates that the inherent consistency within CLIP itself can be effectively leveraged for adjustment.

Moreover, we find that the self-self attention (e.g., K-K attention) proposed in the previous works [4, 25, 29, 46] exhibit insufficient attention activations. Therefore, we further incorporate the similarity map Simi^{mid} to augment the attention operation, as detailed in the following formula. As shown in Figure 5(b), the attention regions now display more extensive and accurate activations.

$$\text{attn_weight} = \text{softmax}(\mathbf{K}\mathbf{K}^\top) + \text{softmax}(\text{Simi}^{mid}) \quad (6)$$

3.4. Multi-level Feature Fusion

Motivated by the effectiveness of multi-level feature aggregation for enriching details [17, 29, 30, 32, 51], we further explore the potential of leveraging CLIP’s multi-level features in a training-free manner. In visual networks, shallower layers typically capture finer spatial details, while deeper layers provide richer high-level semantics. Since the OVS task requires dense visual-text alignment, we believe the key lies in using the final layer for alignment. Therefore, we propose using CLIP’s final layer as the decoder, with preceding layers as the encoder. The decoder performs two forward passes: one with \mathbb{X}^{penul} and the other with features from early layers. This straightforward approach achieves notable improvements, demonstrating that multi-level feature fusion enables better detail capturing.

4. Experiments

4.1. Experiment Settings

Datasets and Metric We conduct comprehensive evaluations on eight commonly used benchmark datasets, which

are grouped into two categories: 1) with a background class, including PASCAL VOC (VOC21) [15], PASCAL Context (Context) [36], and COCO Object (COCO-Obj) [6]; 2) without a background class, including PASCAL VOC20 (VOC20) [15], Cityscapes (City) [11], PASCAL Context59 (Context59) [36], ADE20K (ADE) [60], and COCOStuff (COCO-Stf) [6]. And we evaluate results with the standard *mean-intersection-over-union* (mIoU) as the metric.

Implementation Details In our experiments, we utilize the CLIP [39] with ViT-B/16 and ViT-L/14 architectures. And our code implementation is built on the MMSegmentation [10]. For the evaluation protocol, we adopt the sliding window inference strategy from SCLIP [46]: input images are resized to have a short side of 336 (560 for Cityscapes [11] due to its higher resolution), and the slide inference is conducted with a 224×224 window and a 112×112 stride. No post-processing strategies are applied. Across all datasets, we use the standard ImageNet prompts [39] combined with their category names to construct text descriptions. As our method is training-free, we directly evaluate on the validation sets of all datasets.

Comparison Methods We compare our approach with various training-free methods, including CLIP [39], MaskCLIP [61], ReCo [43], CLIPSurgery [29], GEM [4], SCLIP [46], ClearCLIP [25], CLIP-DINOiser [48], LaVG [22], NACLIP [18], and ProxyCLIP [26]. Additionally, we include comparisons with some weakly-supervised methods, such as GroupViT [52] and TCL [8].

4.2. Main Results

To ensure a fair comparison, we strictly follow the evaluation protocol specified in the Section 4.1 to reproduce all methods. For CLIP-DINOiser [48], we retrain the model using the OpenAI’s pretrained weights. Table 1 presents the comparison of all methods, where our SC-CLIP achieves an average mIoU of 43.9% on CLIP ViT-B/16, setting a new state-of-the-art results across eight benchmarks with an im-

Table 1. Performance comparison of our approach with other methods on eight semantic segmentation benchmarks. For a fair comparison, we reproduce all methods following the evaluation protocol in Section 4.1, considering the different settings used by each method. CLIP-DINOiser[†] denotes our reproduced results using OpenAI’s pretrained weights. We report ProxyCLIP* results using its DINO-B/16 variant.

Method	With a background category			Without background category					Avg.
	VOC21	Context	COCO-Obj	VOC20	City	Context59	ADE	COCO-Stf	
CLIP ViT-B/16									
CLIP [39]	20.8	9.3	8.9	49.1	6.7	11.2	3.2	5.7	14.4
MaskCLIP [61]	51.4	22.5	24.9	62.9	25.6	26.2	12.3	16.9	30.3
ReCo [43]	25.1	19.9	15.7	57.7	21.6	22.3	11.2	14.8	23.5
GroupViT [52]	52.3	18.7	27.5	79.7	18.5	23.4	10.4	15.3	30.7
TCL [8]	51.2	24.3	30.4	77.5	23.5	30.3	14.9	19.6	33.9
CLIPSurgery [29]	55.2	30.3	29.7	77.5	33.1	33.4	16.1	22.2	37.2
LaVG [22]	62.1	31.6	34.2	82.5	26.2	34.7	15.8	23.2	38.8
NACLIP [18]	58.9	32.2	33.2	79.7	35.5	35.2	17.4	23.3	39.4
SCLIP [46]	59.7	31.7	33.5	81.5	32.3	34.5	16.5	22.7	39.1
ClearCLIP [25]	57.0	32.2	32.5	82.3	32.8	35.8	17.3	24.0	39.2
GEM [4]	58.7	32.0	32.9	81.7	32.6	35.6	16.9	23.9	39.3
CLIP-DINOiser [†] [48]	57.8	32.1	32.0	78.0	36.2	36.0	16.8	22.6	38.9
ProxyCLIP* [26]	56.6	34.0	34.6	76.8	37.5	37.4	18.7	25.1	40.1
SC-CLIP (Ours)	64.6	36.8	37.7	84.3	41.0	40.1	20.1	26.6	43.9
CLIP ViT-L/14									
CLIP [39]	10.3	4.5	4.4	19.9	3.2	5.7	1.9	3.2	6.6
MaskCLIP [61]	24.8	9.7	10.2	30.1	12.1	13.0	7.1	9.0	14.5
CLIPSurgery [29]	47.9	27.3	28.1	84.3	29.7	31.0	17.3	21.4	35.9
NACLIP [18]	52.1	28.7	29.9	78.6	31.4	32.1	17.3	21.4	36.4
SCLIP [46]	44.4	22.3	24.9	70.6	21.3	25.2	10.9	16.5	29.5
ClearCLIP [25]	48.6	28.0	28.6	84.8	32.1	31.5	16.9	21.2	36.5
GEM [4]	45.2	25.5	28.3	83.7	27.1	28.1	13.2	19.2	33.8
ProxyCLIP* [26]	58.1	34.1	37.4	82.0	38.1	37.3	21.2	25.5	41.7
SC-CLIP (Ours)	65.0	36.9	40.5	88.3	41.3	40.6	21.7	26.9	45.2

pressive 9.5% improvement over previous methods. On the VOC21 and VOC20 datasets, SC-CLIP achieves 64.6 and 84.3, respectively. Furthermore, our method demonstrates robustness across different backbones, achieving optimal performance on CLIP ViT-L/14 with an average mIoU of 45.2%, improving the results by 3.5% average mIoU.

In contrast to ProxyCLIP [26], which relies on the DINO-B/16 [7] backbone to provide attention weights, our method does not depend on any auxiliary backbone yet achieves superior results. This highlights the inherent properties of CLIP can be effectively leveraged to calibrate itself, thereby enhancing its overall semantic coherence.

The vanilla CLIP [39] achieves only a 14.4% and 6.6% average mIoU on ViT-B/16 and ViT-L/14 respectively, demonstrating its limitations in capturing fine-grained spatial details. Our training-free method boosts performance by threefold on ViT-B/16 and by 6.8 times on ViT-L/14, effectively unlocking CLIP’s inherent potential for dense prediction applications without introducing new data, parameters, or relying on additional backbones.

Table 2. Ablation experiments on the proposed strategies.

Method	V21	C60	Obj	C59	Stf	Avg
baseline	58.2	32.3	34.0	35.4	23.6	36.7
+ AnomRes	60.3	33.3	34.9	36.5	24.3	37.9
+ AttnEnh	61.2	34.2	36.2	37.4	24.9	38.8
+ FeatAgg	62.1	34.8	37.4	38.0	25.7	39.6
+ MultiFuse	64.6	36.8	37.7	40.1	26.6	41.2

4.3. Ablation Study

In this section, we conduct comprehensive ablation experiments to validate the effectiveness of our method. We use SCLIP [46] as our baseline, which modifies the attention mechanism in the final layer by replacing the original Q-K attention with Q-Q and K-K attention, to enhance correlations. Additionally, we remove the residual connections and feed-forward network (FFN) following [25, 26].

Analysis of Various Strategies In Table 2, we incrementally incorporate each strategy to highlight its contribution.

Table 3. Ablation study of resolving the anomaly tokens.

Method	V21	C60	Obj	C59	Stf	Avg
baseline	58.2	32.3	34.0	35.4	23.6	36.7
resolve (1)	58.5	32.6	34.3	35.7	23.9	37.0
resolve (3)	59.2	32.9	34.6	36.0	24.0	37.3
resolve (5)	59.7	33.1	34.7	36.2	24.2	37.6
resolve (10)	60.3	33.3	34.9	36.5	24.3	37.9
resolve (15)	60.3	33.4	34.9	36.6	24.3	37.9

Table 4. Ablation study of self-adjusting strategy.

position	source	V21	C60	C59	Stf	Avg
without		58.2	32.3	35.4	23.6	37.4
\mathbb{X}^{penul}	DINO	58.0	31.8	34.3	23.5	36.9
	4	58.9	32.6	35.2	24.2	37.7
	8	60.1	33.5	36.2	24.5	38.6
	9	60.0	33.4	36.2	24.5	38.5
\mathbb{X}^{last}	DINO	62.6	34.0	37.2	25.4	39.8
	4	61.4	34.2	37.2	25.1	39.5
	5	61.2	34.1	37.1	25.0	39.4
	9	60.1	33.7	36.7	24.7	38.8
both	DINO	58.8	32.0	34.5	23.8	37.3
	(8, 5)	61.7	34.2	37.1	25.1	39.5
	(4, 9)	58.5	32.5	35.1	24.1	37.6
	(9, 4)	62.0	34.4	37.3	25.3	39.8

First, by identifying and resolving the anomaly tokens (denoted by AnomRes), our method achieves a 1.2% mIoU improvement, effectively addressing the issues brought by anomaly tokens, as discussed in Section 3.2. Next, we apply the self-adjusting strategy proposed in Section 3.3, which leverages the spatial consistency within CLIP’s mid-level features to enhance attention correlation (denoted by AttnEnh), leading to a 0.9% improvement. By adaptively aggregating deep features (FeatAgg), we obtain a further 0.8% gain in mIoU. Finally, the multi-level fusion strategy (MultiFuse) introduced in Section 3.4 provides a 1.6% boost in mIoU. Together, these strategies contribute to a substantial 12% improvements over the baseline, significantly improving CLIP’s dense feature representation.

Resolving the Anomaly Tokens As we use the LOF algorithm to identify the anomaly tokens, we need to adjust the contamination hyperparameter to control the number of detected anomalies. We explore the optimal number of tokens to resolve, as shown in Table 3. As the number increases from 1 to 10, performance gradually improves. However,

Table 5. Ablation study of the multi-level fusion strategy.

layer	V21	C60	City	C59	ADE	Stf	Avg
w/o.	62.1	34.8	36.8	38.0	18.9	25.7	36.1
<i>(a) Ours</i>							
{5}	63.9	34.9	41.0	39.2	18.7	26.0	37.3
{9}	65.0	36.4	39.3	39.7	19.8	26.3	37.8
{5, 9}	65.1	36.6	40.6	40.0	19.9	26.4	38.1
4 - 11	63.9	36.4	39.9	39.7	19.9	26.6	37.7
5 - 10	64.4	36.7	40.7	40.0	20.0	26.5	38.1
4 - 10	64.6	36.8	41.0	40.1	20.1	26.6	38.2
<i>(b) Direct Summing Up</i>							
{5, 9}	60.7	29.8	31.4	35.0	15.9	23.8	32.8
4 - 10	19.5	3.5	9.8	15.4	3.6	8.0	10.0
<i>(c) Dual path in CLIPSurgery [29]</i>							
{5, 9}	63.8	35.9	38.1	39.2	19.0	26.2	37.0
4 - 10	63.5	35.4	39.7	38.5	18.6	26.2	37.0

further increasing this number to 15 yields no additional gains. Therefore, we adopt the removal of 10 tokens (about 5% of the ViT-B/16 token sequence) in our method.

Self-adjusting Strategy In Table 4, we conduct a comprehensive analysis of the self-adjusting strategy. We explore different sources to provide similarity map. And we find that adjusting both \mathbb{X}^{penul} and \mathbb{X}^{last} is essential, serving as the pre- and post-adjustment for the last layer. Experiments indicate that using layer 9 for pre-adjustment and layer 4 for post-adjustment yields the optimal results, corresponding to (9, 4) in the table, achieving an average 39.8% mIoU, a 6% improvement over the baseline. We hypothesize that the deeper mid-layers, with their broader activations, aggregate richer semantics that help the attention mechanism capture coherent regions. In contrast, the shallower mid-layer, with more localized activations, focuses on finer details, preserving intricate spatial information. And our method is robust to different combinations, with (8, 5) also achieving an mIoU of 39.5. Additional visualizations are available in the supplementary materials. Furthermore, we compare our approach with DINO, following prior studies [44, 47, 48]. When applied to \mathbb{X}^{last} , DINO shows superior performance, showing its fine-grained details; however, our approach achieves comparable results when both pre- and post-adjustments are applied, fully unlocking CLIP’s potential without relying on additional backbones.

Multi-level Fusion Strategy In Table 5, we conduct various experiments on the multi-level fusion strategy, which leverages intermediate layer features and uses the final layer as a decoder for alignment. We find that adding a single

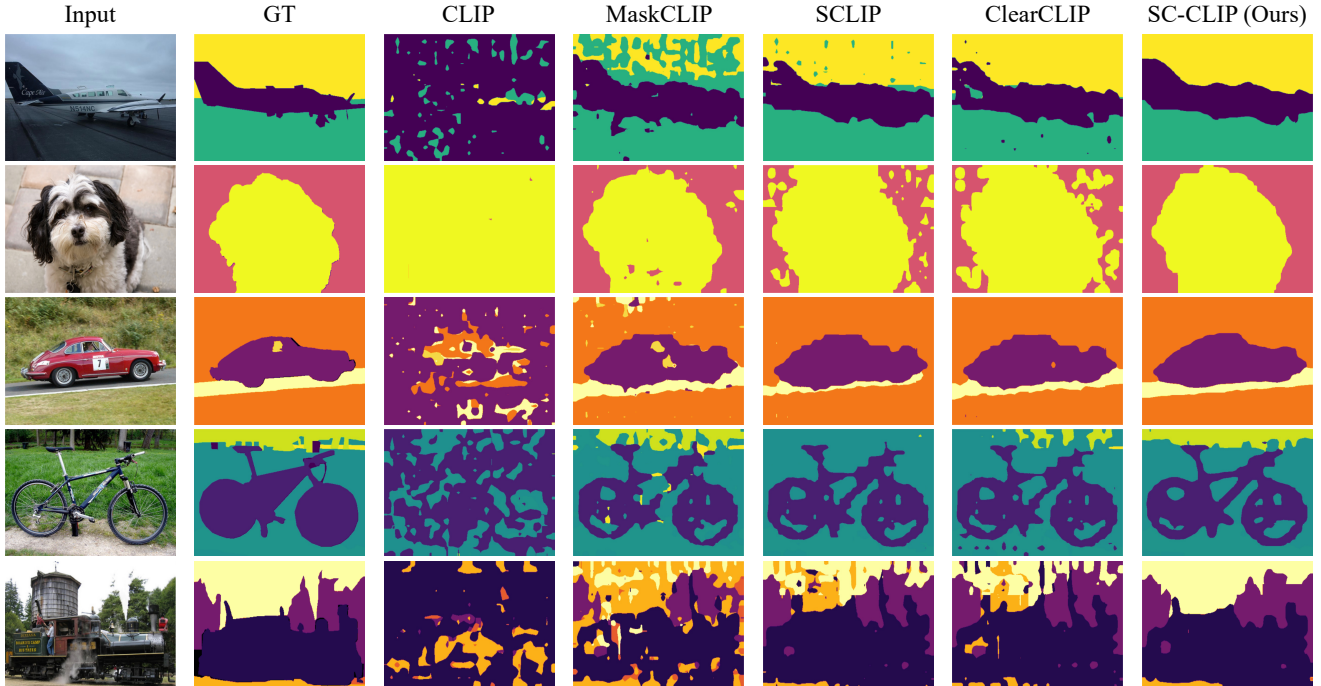


Figure 6. Qualitative Results of Open-Vocabulary Segmentation. We compare our method with CLIP [39], MaskCLIP [61], SCLIP [46] and ClearCLIP [25], all without post-processing. Our SC-CLIP produces much clearer and more accurate segmentation maps.

layer, such as {5} and {9} in the table, already improves performance, with a notable boost on the CityScapes [11] dataset from 36.8 to 41.0. Next, we explore fusing more layers, revealing that our method is robust to the choice of selected layers, as different combinations yield similar improvements. The notation 4–10 in the table indicates fusing all features from layers 4 to 10, and this achieves the best average performance with 38.2% average mIoU, showing the effectiveness of capturing details across various level.

Then we compare different fusion strategies. The first is (b) Direct Summing Up, which directly sums features from different layers. This method severely degrades the performance because of the significant noise in CLIP’s original features. Additionally, we compare with (c) CLIPSurgery’s dual-path strategy [29], which differs from ours by modifying each layer as a decoder and summing up at the end. The results show that our method outperforms them by 1.2% mIoU, which supports our hypothesis that the key is to use the final layer as the decoder for alignment.

Efficiency Comparison We also assess the efficiency of our approach. Compared to the previous best-performing method, ProxyCLIP [26], our approach reduces FLOPs from 34.3G to 17.4G. Additionally, their method increases the model’s parameters count to 235.4M with the DINO-B/16 backbone, while our model retains the original CLIP’s 149.6M parameters. In terms of the inference speed, our approach increases FPS from 10.6 to 15.4 using the sliding-window inference strategy on the VOC20 dataset [15].

4.4. Visualization

In Figure 6, we present the qualitative comparison of CLIP [39], MaskCLIP [61], SCLIP [46], ClearCLIP [25], and our method SC-CLIP. For a fair comparison, we do not use any post-processing technique. The results demonstrate that SC-CLIP consistently achieves higher quality and more precise segmentation maps than the other methods. Notably, the results from vanilla CLIP are considerably noisy and exhibit an over-smoothing effect with global information (e.g., in the second row, the entire image is labeled as “dog”). By performing self-calibration without the need for additional data, parameters, or backbones, SC-CLIP enables CLIP to produce semantically coherent results.

5. Conclusion

In this work, we present Self-Calibrated CLIP (SC-CLIP), a training-free method to enhance the open-vocabulary segmentation performance of CLIP. We first identify and resolve the issues of anomaly tokens, mitigating their negative impact. Then we leverage the semantic consistency within CLIP’s intermediate features to enhance both feature discriminability and attention correlation. Together with multi-level fusion strategy, our SC-CLIP sets new state-of-the-art results across all datasets, without requiring additional data, parameters or backbone. This demonstrates the inherent properties of CLIP can be effectively leveraged to calibrate itself to produce semantically coherent representations.

References

- [1] Hervé Abdi and Lynne J Williams. Principal component analysis. *Wiley interdisciplinary reviews: computational statistics*, 2(4):433–459, 2010. 2
- [2] Stanislaw Antol, Aishwarya Agrawal, Jiasen Lu, Margaret Mitchell, Dhruv Batra, C Lawrence Zitnick, and Devi Parikh. Vqa: Visual question answering. In *ICCV*, pages 2425–2433, 2015. 2
- [3] Luca Barsellotti, Roberto Amoroso, Marcella Cornia, Lorenzo Baraldi, and Rita Cucchiara. Training-free open-vocabulary segmentation with offline diffusion-augmented prototype generation. In *CVPR*, pages 3689–3698, 2024. 3
- [4] Walid Boussethem, Felix Petersen, Vittorio Ferrari, and Hilde Kuehne. Grounding everything: Emerging localization properties in vision-language transformers. In *CVPR*, pages 3828–3837, 2024. 1, 3, 5, 6, 12
- [5] Markus M Breunig, Hans-Peter Kriegel, Raymond T Ng, and Jörg Sander. Lof: identifying density-based local outliers. In *SIGMOD*, pages 93–104, 2000. 2, 3
- [6] Holger Caesar, Jasper Uijlings, and Vittorio Ferrari. Cocostuff: Thing and stuff classes in context. In *CVPR*, pages 1209–1218, 2018. 1, 5, 12
- [7] Mathilde Caron, Hugo Touvron, Ishan Misra, Hervé Jégou, Julien Mairal, Piotr Bojanowski, and Armand Joulin. Emerging properties in self-supervised vision transformers. In *ICCV*, 2021. 1, 3, 4, 6
- [8] Junbum Cha, Jonghwan Mun, and Byungseok Roh. Learning to generate text-grounded mask for open-world semantic segmentation from only image-text pairs. In *CVPR*, 2023. 2, 5, 6
- [9] Seokju Cho, Heeseong Shin, Sunghwan Hong, Anurag Arnab, Paul Hongsuck Seo, and Seungryong Kim. Cat-seg: Cost aggregation for open-vocabulary semantic segmentation. In *CVPR*, pages 4113–4123, 2024. 2
- [10] MMsegmentation Contributors. Mmsegmentation: Openmmlab semantic segmentation toolbox and benchmark, 2020. 5
- [11] Marius Cordts, Mohamed Omran, Sebastian Ramos, Timo Rehfeld, Markus Enzweiler, Rodrigo Benenson, Uwe Franke, Stefan Roth, and Bernt Schiele. The cityscapes dataset for semantic urban scene understanding. In *CVPR*, 2016. 5, 8
- [12] Timothée Darcet, Maxime Oquab, Julien Mairal, and Piotr Bojanowski. Vision transformers need registers. In *ICLR*, 2024. 3
- [13] Jian Ding, Nan Xue, Gui-Song Xia, and Dengxin Dai. Decoupling zero-shot semantic segmentation. In *CVPR*, 2022. 2
- [14] Alexey Dosovitskiy, Lucas Beyer, Alexander Kolesnikov, Dirk Weissenborn, Xiaohua Zhai, Thomas Unterthiner, Mostafa Dehghani, Matthias Minderer, Georg Heigold, Sylvain Gelly, Jakob Uszkoreit, and Neil Houlsby. An image is worth 16x16 words: Transformers for image recognition at scale. In *ICLR*, 2021. 3
- [15] Mark Everingham and John Winn. The pascal visual object classes challenge 2012 (voc2012) development kit. *Pattern Anal. Stat. Model. Comput. Learn., Tech. Rep.*, 2007(1-45):5, 2012. 5, 8
- [16] Golnaz Ghiasi, Xiuye Gu, Yin Cui, and Tsung-Yi Lin. Scaling open-vocabulary image segmentation with image-level labels. In *ECCV*, pages 540–557, 2022. 2
- [17] Meng-Hao Guo, Cheng-Ze Lu, Qibin Hou, Zhengning Liu, Ming-Ming Cheng, and Shi-Min Hu. Segnext: Rethinking convolutional attention design for semantic segmentation. In *NeurIPS*, pages 1140–1156, 2022. 5
- [18] Sina Hajimiri, Ismail Ben Ayed, and Jose Dolz. Pay attention to your neighbours: Training-free open-vocabulary semantic segmentation. In *WACV*, 2025. 1, 3, 5, 6
- [19] Kunyang Han, Yong Liu, Jun Hao Liew, Henghui Ding, Jiajun Liu, Yitong Wang, Yansong Tang, Yujiu Yang, Jiashi Feng, Yao Zhao, et al. Global knowledge calibration for fast open-vocabulary segmentation. In *ICCV*, pages 797–807, 2023. 2
- [20] Wenbin He, Suphanut Jamonnak, Liang Gou, and Liu Ren. Clip-s4: Language-guided self-supervised semantic segmentation. In *CVPR*, pages 11207–11216, 2023. 2
- [21] Chao Jia, Yinfei Yang, Ye Xia, Yi-Ting Chen, Zarana Parekh, Hieu Pham, Quoc Le, Yun-Hsuan Sung, Zhen Li, and Tom Duerig. Scaling up visual and vision-language representation learning with noisy text supervision. In *ICML*, 2021. 2
- [22] Dahyun Kang and Minsu Cho. In defense of lazy visual grounding for open-vocabulary semantic segmentation. In *ECCV*, 2024. 1, 3, 5, 6
- [23] Aisha Urooj Khan, Hilde Kuehne, Chuang Gan, Niels Da Victoria Lobo, and Mubarak Shah. Weakly supervised grounding for vqa in vision-language transformers. In *ECCV*, pages 652–670. Springer, 2022. 2
- [24] Alexander Kirillov, Eric Mintun, Nikhila Ravi, Hanzi Mao, Chloe Rolland, Laura Gustafson, Tete Xiao, Spencer Whitehead, Alexander C Berg, Wan-Yen Lo, et al. Segment anything. In *ICCV*, pages 4015–4026, 2023. 1, 3
- [25] Mengcheng Lan, Chaofeng Chen, Yiping Ke, Xinjiang Wang, Litong Feng, and Wayne Zhang. Clearclip: Decomposing clip representations for dense vision-language inference. In *ECCV*, 2024. 1, 3, 5, 6, 8, 12, 13
- [26] Mengcheng Lan, Chaofeng Chen, Yiping Ke, Xinjiang Wang, Litong Feng, and Wayne Zhang. Proxyclick: Proxy attention improves clip for open-vocabulary segmentation. In *ECCV*, 2024. 1, 3, 4, 5, 6, 8, 11, 12
- [27] Boyi Li, Kilian Q. Weinberger, Serge J. Belongie, Vladlen Koltun, and René Ranftl. Language-driven semantic segmentation. In *ICLR*, 2022. 2
- [28] Junnan Li, Dongxu Li, Caiming Xiong, and Steven Hoi. Blip: Bootstrapping language-image pre-training for unified vision-language understanding and generation. In *ICML*, pages 12888–12900, 2022. 2
- [29] Yi Li, Hualiang Wang, Yiqun Duan, and Xiaomeng Li. Clip surgery for better explainability with enhancement in open-vocabulary tasks. *arXiv preprint arXiv:2304.05653*, 2023. 1, 3, 5, 6, 7, 8, 12
- [30] Yunheng Li, Zhongyu Li, Quansheng Zeng, Qibin Hou, and Ming-Ming Cheng. Cascade-clip: Cascaded vision-language embeddings alignment for zero-shot semantic segmentation. In *ICML*, 2024. 5

- [31] Feng Liang, Bichen Wu, Xiaoliang Dai, Kunpeng Li, Yinan Zhao, Hang Zhang, Peizhao Zhang, Peter Vajda, and Diana Marculescu. Open-vocabulary semantic segmentation with mask-adapted clip. In *CVPR*, pages 7061–7070, 2023. 2
- [32] Tsung-Yi Lin, Piotr Dollár, Ross Girshick, Kaiming He, Bharath Hariharan, and Serge Belongie. Feature pyramid networks for object detection. In *CVPR*, 2017. 5
- [33] Yong Liu, Sule Bai, Guanbin Li, Yitong Wang, and Yansong Tang. Open-vocabulary segmentation with semantic-assisted calibration. In *CVPR*, pages 3491–3500, 2024. 2
- [34] Huaishao Luo, Junwei Bao, Youzheng Wu, Xiaodong He, and Tianrui Li. Segclip: Patch aggregation with learnable centers for open-vocabulary semantic segmentation. In *ICML*, 2023. 2
- [35] Anand Mishra, Karteek Alahari, and CV Jawahar. Image retrieval using textual cues. In *ICCV*, 2013. 2
- [36] Roozbeh Mottaghi, Xianjie Chen, Xiaobai Liu, Nam-Gyu Cho, Seong-Whan Lee, Sanja Fidler, Raquel Urtasun, and Alan Yuille. The role of context for object detection and semantic segmentation in the wild. In *CVPR*, 2014. 5
- [37] Jishnu Mukhoti, Tsung-Yu Lin, Omid Poursaeed, Rui Wang, Ashish Shah, Philip HS Torr, and Ser-Nam Lim. Open vocabulary semantic segmentation with patch aligned contrastive learning. In *CVPR*, pages 19413–19423, 2023. 2
- [38] Jie Qin, Jie Wu, Pengxiang Yan, Ming Li, Ren Yuxi, Xuefeng Xiao, Yitong Wang, Rui Wang, Shilei Wen, Xin Pan, et al. Freeseg: Unified, universal and open-vocabulary image segmentation. In *CVPR*, pages 19446–19455, 2023. 2
- [39] Alec Radford, Jong Wook Kim, Chris Hallacy, Aditya Ramesh, Gabriel Goh, Sandhini Agarwal, Girish Sastry, Amanda Askell, Pamela Mishkin, Jack Clark, et al. Learning transferable visual models from natural language supervision. In *ICML*, 2021. 1, 2, 5, 6, 8, 12, 13
- [40] Pengzhen Ren, Changlin Li, Hang Xu, Yi Zhu, Guangrun Wang, Jianzhuang Liu, Xiaojun Chang, and Xiaodan Liang. Viewco: Discovering text-supervised segmentation masks via multi-view semantic consistency. In *ICLR*, 2023. 2
- [41] Robin Rombach, Andreas Blattmann, Dominik Lorenz, Patrick Esser, and Björn Ommer. High-resolution image synthesis with latent diffusion models. In *CVPR*, 2022. 1
- [42] Tong Shao, Zhuotao Tian, Hang Zhao, and Jingyong Su. Explore the potential of clip for training-free open vocabulary semantic segmentation. *arXiv preprint arXiv:2407.08268*, 2024. 1, 3
- [43] Gyungin Shin, Weidi Xie, and Samuel Albanie. Reco: Retrieve and co-segment for zero-shot transfer. In *NeurIPS*, 2022. 5, 6
- [44] Oriane Siméoni, Gilles Puy, Huy V. Vo, Simon Roburin, Spyros Gidaris, Andrei Bursuc, Patrick Pérez, Renaud Marlet, and Jean Ponce. Localizing objects with self-supervised transformers and no labels. In *BMVC*, page 310, 2021. 7, 11
- [45] Ashish Vaswani, Noam Shazeer, Niki Parmar, Jakob Uszkoreit, Llion Jones, Aidan N Gomez, Łukasz Kaiser, and Illia Polosukhin. Attention is all you need. In *NeurIPS*, 2017. 3
- [46] Feng Wang, Jieru Mei, and Alan Yuille. Sclip: Rethinking self-attention for dense vision-language inference. In *ECCV*, pages 315–332, 2024. 1, 3, 5, 6, 8, 12, 13
- [47] Yangtao Wang, Xi Shen, Shell Xu Hu, Yuan Yuan, James L Crowley, and Dominique Vaufreydaz. Self-supervised transformers for unsupervised object discovery using normalized cut. In *CVPR*, pages 14543–14553, 2022. 7, 11
- [48] Monika Wyszoczańska, Oriane Siméoni, Michaël Ramamonjisoa, Andrei Bursuc, Tomasz Trzciniński, and Patrick Pérez. Clip-dinoiser: Teaching clip a few dino tricks. In *ECCV*, 2024. 1, 3, 4, 5, 6, 7, 11
- [49] Guangxuan Xiao, Yuandong Tian, Beidi Chen, Song Han, and Mike Lewis. Efficient streaming language models with attention sinks. In *ICLR*, 2024. 3
- [50] Bin Xie, Jiale Cao, Jin Xie, Fahad Shahbaz Khan, and Yanwei Pang. Sed: A simple encoder-decoder for open-vocabulary semantic segmentation. In *CVPR*, pages 3426–3436, 2024. 2
- [51] Enze Xie, Wenhai Wang, Zhiding Yu, Anima Anandkumar, Jose M. Alvarez, and Ping Luo. Segformer: Simple and efficient design for semantic segmentation with transformers. In *NeurIPS*, 2021. 5
- [52] Jiarui Xu, Shalini De Mello, Sifei Liu, Wonmin Byeon, Thomas Breuel, Jan Kautz, and Xiaolong Wang. Groupvit: Semantic segmentation emerges from text supervision. In *CVPR*, 2022. 2, 5, 6
- [53] Jilan Xu, Junlin Hou, Yuejie Zhang, Rui Feng, Yi Wang, Yu Qiao, and Weidi Xie. Learning open-vocabulary semantic segmentation models from natural language supervision. In *CVPR*, 2023. 2
- [54] Jiarui Xu, Sifei Liu, Arash Vahdat, Wonmin Byeon, Xiaolong Wang, and Shalini De Mello. Open-vocabulary panoptic segmentation with text-to-image diffusion models. In *CVPR*, pages 2955–2966, 2023. 2
- [55] Mengde Xu, Zheng Zhang, Fangyun Wei, Yutong Lin, Yue Cao, Han Hu, and Xiang Bai. A simple baseline for open-vocabulary semantic segmentation with pre-trained vision-language model. In *ECCV*, pages 736–753, 2022.
- [56] Mengde Xu, Zheng Zhang, Fangyun Wei, Han Hu, and Xiang Bai. Side adapter network for open-vocabulary semantic segmentation. In *CVPR*, pages 2945–2954, 2023.
- [57] Xin Xu, Tianyi Xiong, Zheng Ding, and Zhuowen Tu. Masq-clip for open-vocabulary universal image segmentation. In *ICCV*, pages 887–898, 2023.
- [58] Qihang Yu, Ju He, Xueqing Deng, Xiaohui Shen, and Liang-Chieh Chen. Convolutions die hard: Open-vocabulary segmentation with single frozen convolutional clip. In *NeurIPS*, pages 32215–32234, 2023. 2
- [59] Fei Zhang, Tianfei Zhou, Boyang Li, Hao He, Chaofan Ma, Tianjiao Zhang, Jiangchao Yao, Ya Zhang, and Yanfeng Wang. Uncovering prototypical knowledge for weakly open-vocabulary semantic segmentation. In *NeurIPS*, pages 73652–73665, 2023. 3
- [60] Bolei Zhou, Hang Zhao, Xavier Puig, Sanja Fidler, Adela Barriuso, and Antonio Torralba. Scene parsing through ADE20K dataset. In *CVPR*, 2017. 4, 5
- [61] Chong Zhou, Chen Change Loy, and Bo Dai. Extract free dense labels from clip. In *ECCV*, pages 696–712, 2022. 1, 3, 5, 6, 8, 12, 13

Self-Calibrated CLIP for Training-Free Open-Vocabulary Segmentation

Supplementary Material

6. More Implementation Details

After deriving the similarity map Simi^{mid} from CLIP’s mid-level layers, we apply thresholding following previous methods [44, 47, 48]. Specifically, values below the threshold β are set to zero to strengthen feature correlation. And we set β to 0.4. When leveraging Simi^{mid} to enhance attention, we follow prior works [26] by masking the similarity map, setting values below zero to negative infinity. For the experiments with CLIP ViT-L/14, the hyperparameters are configured as follows: resolving 10 anomaly tokens, using the 17th-layer features for pre-adjustment, the 7th-layer features for post-adjustment, and integrating features from the 9th to 20th layers as multi-level fusion.

7. Various Interpolation Methods

We explore various interpolation methods in Table 6. After identifying 10 anomaly tokens, we conduct experiments using bilinear interpolation, nearest neighbor interpolation, median interpolation (replacing with the median value of neighboring pixels), weighted interpolation (assigning weights based on distance), and mean interpolation. The implementations align with the description in Section 3.2, ensuring that anomaly tokens in the neighborhood are excluded from the calculations. Our findings indicate that all interpolation methods enhance performance, with only minor differences in their effectiveness. Among these, mean interpolation yields the best results, achieving an average mIoU of 37.9%. Consequently, we adopt mean interpolation as the method for our approach.

Table 6. Ablation study of various interpolation methods.

Method	V21	C60	Obj	C59	Stf	Avg
baseline	58.2	32.3	34.0	35.4	23.6	36.7
bilinear	59.9	33.2	34.6	36.3	24.1	37.6
nearest	60.1	33.2	34.7	36.3	24.1	37.7
median	60.3	33.2	34.8	36.5	24.3	37.8
weighted	60.1	33.3	34.8	36.4	24.3	37.8
mean	60.3	33.3	34.9	36.5	24.3	37.9

8. Self-Adjusting Strategy

In Section 4.3, we emphasize that adjusting both \mathbb{X}^{penul} and \mathbb{X}^{last} is crucial, acting as the pre- and post-adjustment for the final layer. Our experiments further demonstrate that employing a deeper mid-layer (e.g., 9) for pre-adjustment and a shallower mid-layer (e.g., 4) for post-adjustment yields superior results. As illustrated in Figure 7, we visualize three examples, revealing that shallower layers ex-

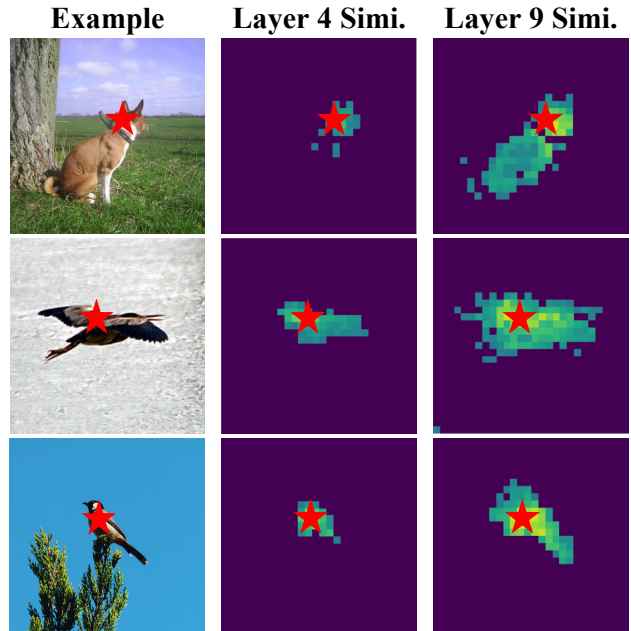


Figure 7. Visualization of shallower and deeper mid-layer patch similarity. \star denotes the selected token.

Table 7. More ablation study of self-adjusting strategy.

position	source	V21	C60	C59	Stf	Avg
without		58.2	32.3	35.4	23.6	37.4
both	(5, 8)	59.8	33.0	35.7	24.4	38.2
	(4, 9)	58.5	32.5	35.1	24.1	37.6
	(10, 4)	61.6	33.3	36.4	24.8	39.0
	(8, 5)	61.7	34.2	37.1	25.1	39.5
	(9, 5)	61.6	34.2	37.1	25.1	39.5
	(9, 4)	62.0	34.4	37.3	25.3	39.8

hibit more localized activations, while deeper layers provide broader activations. We hypothesize that deeper mid-layers are well-suited for pre-adjustment due to their broader activations, which help aggregate more regions and enable the attention mechanism in the final layer to capture more coherent semantics. In contrast, shallower mid-layers are ideal for post-adjustment, as their localized activations can preserve intricate spatial information. Additionally, we conduct more experiments as summarized in Table 7. We find that various combinations consistently enhance performance, underscoring the robustness of our approach.

9. Different Correlative Self-attention

In the main text, our baseline builds on the K-K form of correlative self-attention, replacing the original Q-K atten-

Table 8. Ablation experiments on various self-self attention.

Corr. Attn.	V21	C60	Obj	C59	Stf	Avg
V-V	63.5	36.3	36.9	39.6	26.2	40.5
Q-Q	63.8	36.5	37.6	39.9	26.6	40.9
{Q-Q}+{K-K}	64.2	36.5	37.5	39.8	26.3	40.9
K-K	64.6	36.8	37.7	40.1	26.6	41.2

tion of CLIP. To explore alternative forms of correlative self-attention, we evaluate several approaches, including Q-Q [25], V-V [29], and a combination of Q-Q and K-K [46]. As summarized in Table 8, different correlative attention mechanisms achieve comparable performance, with the K-K approach yielding the best results. The final model achieves an average performance of 41.2% mIoU.

10. Efficiency Comparison

We conduct an efficiency comparison across different training-free OVS methods. All experiments are conducted under the same hardware conditions, using the sliding-window inference strategy described in the main text, with the COCO-Object dataset [6]. As shown in Table 9, our method, SC-CLIP, maintains comparable FPS to vanilla CLIP while achieving lower FLOPs due to the removal of the FFN network. Besides, SC-CLIP significantly outperforms the vanilla CLIP’s performance by threefold. Compared to ProxyCLIP [26], SC-CLIP does not rely on additional backbones, significantly improving the efficiency. Specifically, the FPS increases from 4.1 to 9.8, and FLOPs are reduced from 34.3 to 17.4. Moreover, SC-CLIP also outperforms ProxyCLIP in terms of performance, with the average mIoU increasing from 40.1 to 43.9.

Table 9. Efficiency comparison of training-free methods.

Models	FLOPs ↓ (G)	Params ↓ (M)	Speed ↑ (FPS)	Perf ↑ (mIoU)
CLIP [39]	17.7	149.6	12.2	14.6
MaskCLIP [61]	17.6	149.6	12.1	30.3
CLIPSurgery [29]	18.2	149.6	11.1	37.2
SCLIP [46]	17.7	149.6	12.0	39.1
GEM [4]	18.9	149.6	9.3	39.3
ProxyCLIP [26]	34.3	235.4	4.1	40.1
SC-CLIP (Ours)	17.4	149.6	9.8	43.9

11. Detailed ROC Curve Analysis

We conduct a more detailed analysis of the ROC curves presented in Section 3.3. As shown in Figure 8, the final layer of vanilla CLIP demonstrates poor semantic coherence (AUC=0.66), whereas the mid-layer features of CLIP (AUC=0.76) and DINO features (AUC=0.77) exhibit signif-

icantly better consistency. Applying the baseline outlined in the ablation study improves the AUC of CLIP’s final layer to 0.69. Resolving anomaly tokens increases the AUC to 0.74. Introducing the self-adjusting strategy further enhances the AUC to 0.8, and with the addition of multi-level fusion, the AUC reaches 0.81, surpassing the vanilla CLIP’s AUC by 22.7%. These results clearly demonstrate the effectiveness of our proposed method.

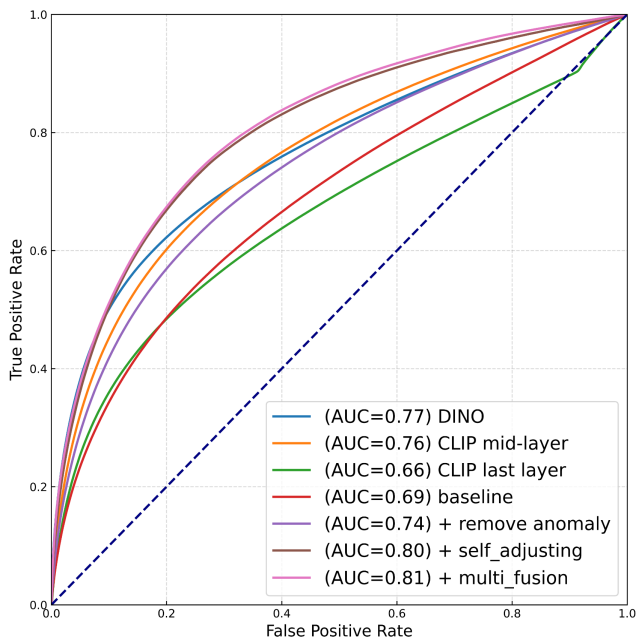


Figure 8. Detailed ROC Curve Analysis.

12. More Visualization Results

Figure 10 presents more visualizations showcasing images from various datasets. We compare the performance of CLIP, MaskCLIP, SCLIP, ClearCLIP, and our proposed method, SC-CLIP. The results clearly demonstrate that SC-CLIP consistently delivers higher-quality and more accurate segmentation maps compared to the other approaches.

We also evaluate the ability of the open-vocabulary task to handle arbitrary language prompts, as illustrated in Figure 9. The method can segment the person in the image using either “Person” and “Skiing Person” as inputs. Notably, we observe that providing more detailed descriptions result in more accurate segmentation outcomes.

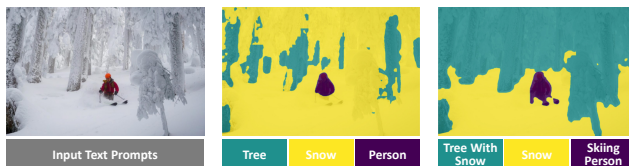


Figure 9. Illustration of segmentation with arbitrarily flexible language guidance. With more detailed descriptions, the segmentation results become more accurate and clearer.

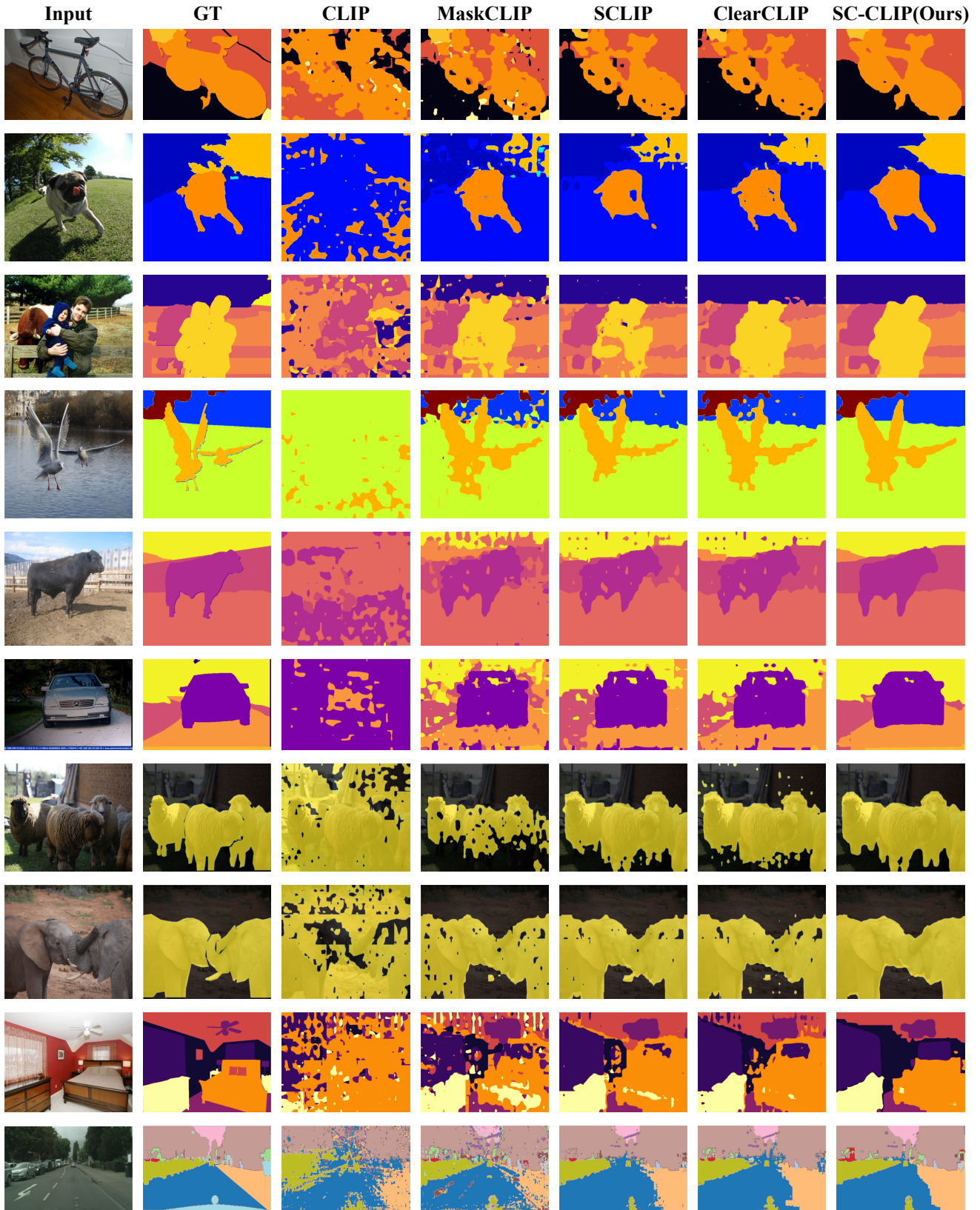


Figure 10. More Open-Vocabulary Segmentation Results. We compare our method with CLIP [39], MaskCLIP [61], SCLIP [46] and ClearCLIP [25], all without post-processing. Our SC-CLIP produces much clearer and more accurate segmentation maps.